



DETERMINATION OF FREQUENCY RESPONSE FUNCTIONS FROM RESPONSE MEASUREMENTS—II. REGENERATION OF FREQUENCY RESPONSE FUNCTIONS FROM POLES AND ZEROS

Y. GAO AND R. B. RANDALL

*School of Mechanical and Manufacturing Engineering, University of New South Wales,
Sydney 2052, Australia*

(Received March 1995; accepted September 1995)

This paper proposes a complete method to track changes in a frequency response function (FRF) which might be caused by a variety of reasons such as the development of local material damage. The changes are tracked in response measurements, without the necessity of measuring the forcing function, but would allow better estimates to be made of this forcing function by an inverse filtering process (as compared with assuming that the FRF is unchanged). The changes in the FRF are obtained in terms of the poles and zeros rather than the more common pole/residue model, using a cepstral curve fitting process as described in a companion paper. The effect of out-of-band modes on the in-band FRF, during such development, is investigated. It is found that they basically determine the slope of the FRF and that a magnitude equaliser in the form of a group of 'phantom zeros' may be applied unchanged over a range of FRF variation. This magnitude equaliser may be determined either from a finite element model or from initial measurements of the FRF where the force is measured. Such measurements might be made under somewhat different conditions, such as on a stationary machine, after which the process described here could be used to update the FRF estimate under operating conditions. The method used to track the changes in the poles and zeros (via the cepstrum) loses information on scaling, and so three scaling methods are introduced and compared. It is next discussed how to combine the tracked in-band poles and zeros with the magnitude equaliser to regenerate a revised FRF as changes proceed. A free-free beam was chosen as the object of study. A slot was cut in the middle of the beam with depth varying in steps up to more than half the thickness to simulate the gradual development of changes in natural frequencies up to 10 per cent. The position of the slot was chosen so that only the symmetric modes changed in frequency, while the antisymmetric modes remained unchanged, and the method was able to reproduce the modified FRFs fully.

© 1996 Academic Press Limited

1. INTRODUCTION

There are a number of situations where it is difficult or impossible to measure forcing functions in operating machines, but where a knowledge of such forcing functions is desirable for diagnostic and other reasons. An example is the case of gearboxes, where it is extremely difficult to measure the force at the gear mesh which is roughly fixed in space, but moving with respect to the meshing gears. Another is the possibility of determining the cylinder pressure in an internal combustion (IC) engine from measurements of external acceleration, without the need to use an inserted pressure transducer. In the companion paper [4], a method was outlined for the determination of the poles and zeros

corresponding to the frequency response function (FRF) of a signal transmission path from response measurements alone, without the need to measure the forcing function. When combined with other information such as the residual effects of out-of-band modes, and scaling, an estimate of the current FRF can be made which can be used in an inverse filtering process to predict the forcing function from the measured responses.

Another potential use for such techniques is the determination of modal properties of structures where it is difficult to apply or measure a forcing function, such as in the case of large structures, rail vehicles, ships, etc., but where the excitation in service is known in general terms or can be adjusted to have suitable characteristics. The requirement of the technique proposed here is that the source is impulsive, so that its spectrum is relatively smooth and flat in the frequency range of interest, but it can be repeated or periodic, giving a well-defined structure which can be isolated in the response cepstrum.

The results in this paper are based on measurements made on a free-free beam using hammer excitation, and further work would be required to extend them to the above applications, but it is thought that the present results demonstrate the potential of the method.

An FRF in a given frequency band can be expressed by a truncated pole/zero model cascaded with a group of 'phantom zeros' [1–3]. These 'phantom zeros' are not associated with the true physical model within the frequency band of interest, but necessary to compensate for the contributions of out-of-band modes. It has been found that the peak and valley positions of the FRFs regenerated using the truncated pole/zero model correspond exactly to their actual positions, but the general slope of such regenerated (log) FRFs is greatly distorted [1, 2]. Figure 1 shows a typical example. Here the dashed curves are the actually measured (log) FRFs (at points 1, 5 and 8 on a free-free beam, see Fig. 3), and the solid ones are regenerated using the poles and zeros in the frequency band 0–3200 Hz (scaled to the mean dB values of their corresponding measured FRFs for comparison) [1].

The contribution of the truncated modes may be expressed in the form of the log spectrum as:

$$\begin{aligned}
 T(\omega) = & -20 \sum_{k \geq N_t + 1} \log |(j\omega - s_k)(j\omega - s_k^*)| + 20 \sum_{k \geq M_c + 1} \log |(j\omega - s_{zk})(j\omega - s_{zk}^*)| \\
 & + 10 \sum_{k \geq M_r + 1} \log (\omega^2 + \sigma_{zk}^2)
 \end{aligned} \tag{1}$$

where s_k and s_{zk} are the out-of-band complex conjugate poles and zeros, respectively, and σ_{zk} , the real zeros on the damping axis [1]. It is shown in [1] and [2] that these contributions can be approximated by a group of 'phantom zeros' within the frequency band considered.

$T(\omega)$ contributes mainly to the general slopes of the in-band (log) FRFs and the contribution would remain nearly unchanged with local material damage, at least up to a certain extent of change in modal properties where the mode shapes before and after damage are still similar to one another. A small shift of the poles and zeros in equation (1) along the frequency axis, say, less than 10 per cent, might correspond to a very serious damage (e.g. a very deep slot in a beam, see later). However, because of the properties of the log function, $T(\omega)$ varies very slowly and smoothly when the test frequency ω is far from the out-of-band poles and zeros. The small relative shifts of these poles and zeros would not cause appreciable in-band variation of $T(\omega)$. The in-band effects of the real-valued zero terms in the equation can usually be neglected because their locations far from the frequency axis are primarily dependent on the damping properties [1, 2] (which

do not affect the slope). Based on the above argument (this point will be verified later), it is proposed that for many of the practical applications envisaged here, it would be possible to have an original model based on the true FRF obtained by actual prior measurements or from a finite element model, which would then be updated by means of cascading the original set of 'phantom zeros' with the actual in-band poles and zeros, updated by curve-fitting the corresponding complex or differential cepstra obtained from response measurements [1–4]. Figure 2 sketches the basic procedure.

In part I [4] the application of two alternative methods to extract poles and zeros from response measurements was discussed, viz. the non-linear least squares (NLLS) and Ibrahim time domain (ITD) methods. The discussion includes the choice of the three weighting functions shown in the figure, which can be used to exclude extraneous information resulting from a repeated or periodic force. In reference [2] the following is discussed: (a) determination of 'phantom zeros' based on an actual pre-measurement of the true FRF using the standard rational fraction polynomial (RFP) curve-fitter [5] and (b) reconstruction of an FRF by cascading the truncated pole/zero model with a magnitude equaliser formed from the group of predetermined 'phantom zeros'. In the current paper, a brief discussion is presented as to how to track the changes in the true in-band pole and zero positions with damage development, but particular emphasis is on the regeneration

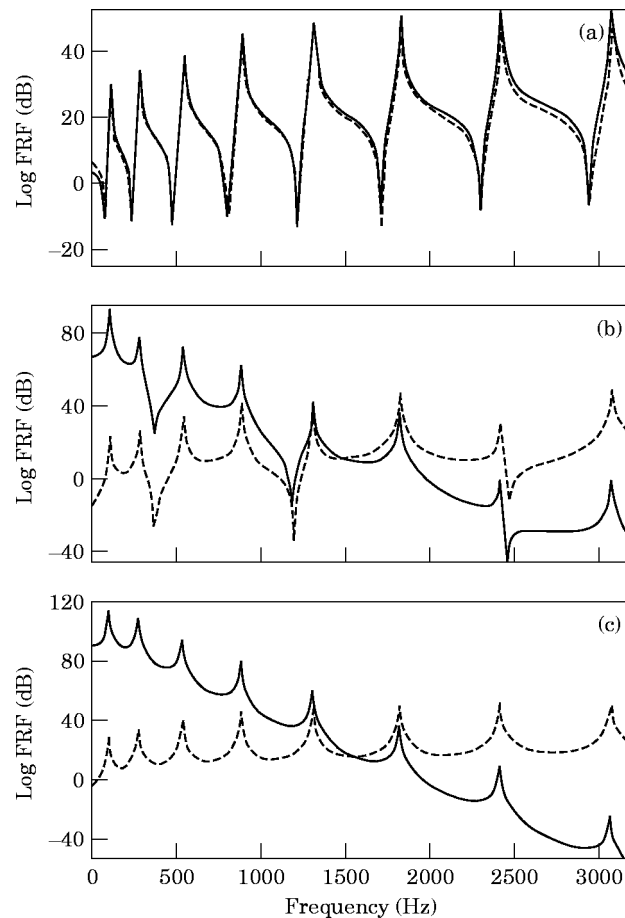


Figure 1. Magnitude distortion caused by truncation. (a) Point 1; (b) point 5; (c) point 8, —, Regenerated; ---, measured.

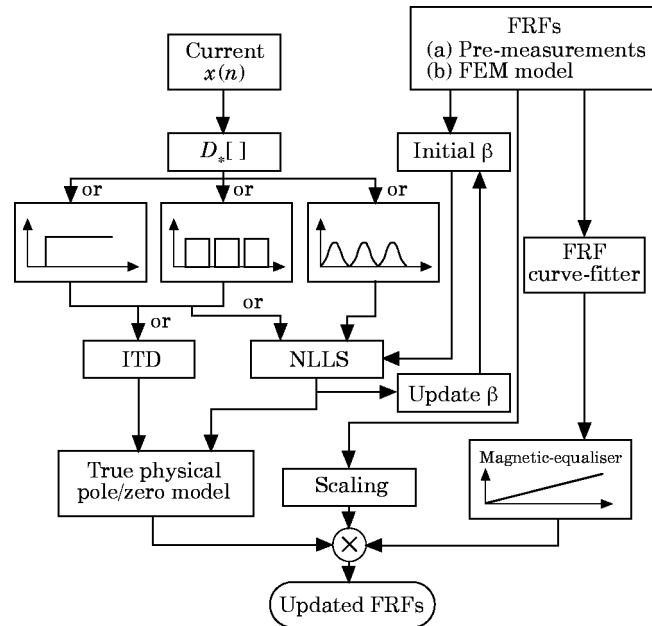


Figure 2. Flow chart of regeneration of FRF from poles and zeros.

of estimated FRFs from the tracked poles and zeros, which involves the determination of scaling factors and magnitude equalisers, as shown in Fig. 2. The phantom zeros constituting the magnitude equaliser can alternatively be obtained from a finite element model, when it is not possible to make an initial true measurement where the force signal is measured.

Much effort has been made in the past to investigate how to predict the location and extent of damage from the changes in model parameters. Yang and Vandiver detected the damage in offshore structures in terms of the relative change amongst the different modal natural frequencies [6, 7]. Thomson explored the influence of a small slot on the free vibration characteristics of uniform cantilever beams [8]. Joshi modelled the local material damage of beams as an effective reduction in Young's modulus to investigate the relation between the damage location and size, and the modal parameter change for different boundary conditions [9]. Yuen used a finite element model of a cantilever beam (which was composed of 15 equal length Timoshenko beam elements), to investigate the change of modal parameters relative to the location and extent of damage [10].

The changes in the FRFs to be detected here are not necessarily due to development of material damage, however, and this is not the main aim of the procedure. An equally important application would be to adapt to changes brought about by different operating conditions of a machine, for example to update measurements made on a stationary gearbox to when it is in operation. Another would be to measure the variation in the modal properties of a number of objects made to the same design, and which would have identical properties in terms of a finite element model.

Here, a free-free beam (1000 mm long and 19 mm square) was chosen as the object of study. A slot 2.5 mm wide was cut in the middle of the beam from 0 to 10 mm in depth with 2 mm increments to give a gradual change in the FRFs. Figure 3 shows the procedure of the slot development. The loss of mass from each cut can be neglected compared with the total mass of the beam. The results from three typical measurement points are

discussed. One (point 1) is the driving point at one end of the beam, another point (point 5) is near the middle of the beam and the third (point 8) is at the other end, as shown in Fig. 3.

2. TRACKING THE SHIFT OF POLE AND ZERO POSITIONS BY CURVE-FITTING RESPONSE CEPSTRA

The NLLS and ITD methods were used to track the changes in in-band pole and zero positions, as described in Part I [4]. For the NLLS procedure, the number of poles and zeros and a trial vector of them can be specified from pre-measurements on the object of study [1] or an FEM model (see later). This trial vector can be used to track the initial changes in modal parameters after which it should be updated using the tracked poles and zeros recursively as damage develops. In this way a series of good trial vectors can be obtained because the damage develops very slowly and the shifts of poles and zeros are small. For the ITD method, however, neither the number of poles and zeros nor their trial vector need be specified, but multiple point measurements are required in order to separate poles from zeros [4]. In tracking the change of pole and zero positions, there is no difference in principle between the two methods. For conciseness, the results from one of them, the NLLS method, will be used here.

The measured response acceleration data were transformed to the response cepstrum data, which were input to the NLLS curve-fitter where the poles and zeros were extracted and then the new initial vector β updated with the extracted poles and zeros, as shown in Fig. 2.

Figure 4 illustrates the goodness of fit in the complex cepstrum curve-fitting. The solid curve is regenerated from the tracked poles and zeros when the slot is 10 mm deep, and the dashed one measured directly.

Table 1 lists the tracked poles with the slot development. It can be seen that the tendency is for the poles of the symmetric modes (corresponding to odd numbers in the table) to shift left of their original positions (no slot in the beam) and for those of antisymmetric modes (corresponding to even numbers in the table) to remain unchanged. This phenomenon is caused by the special position of the slot, which is located at the middle of the beam. For symmetric modes, the slot is at a point of maximum curvature of the beam, where both the bending moment caused by vibration and the reduction of the bending stiffness caused by the slot become maximum, while for the antisymmetric modes, the slot is at a node of the mode shape where the bending moment is zero and the motion is not affected by the reduction of the bending stiffness.

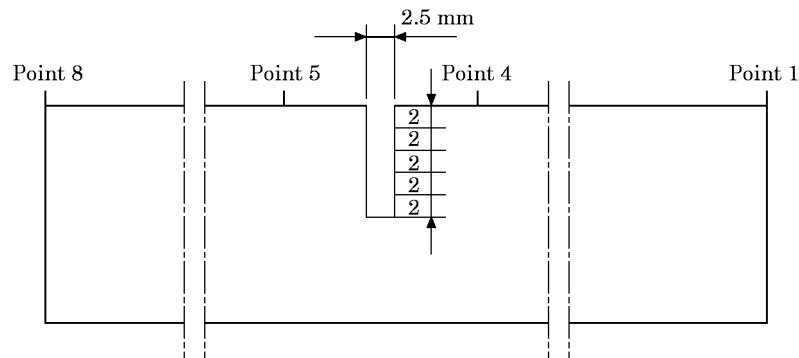


Figure 3. Development of the slot in the free-free beam.

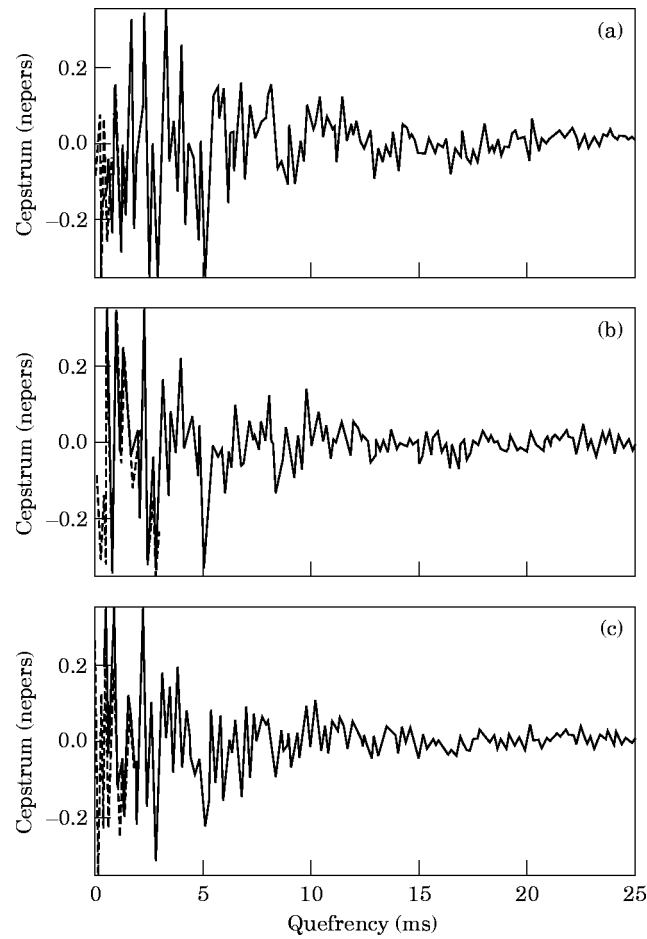


Figure 4. Correspondence between the measured, --- and regenerated, — complex cepstra for a 10-mm deep slot. (a) Point 1; (b) point 5; (c) point 8.

Figure 5 shows the relative shift of the symmetric modes with the slot development. This falls in the range of $6 \sim 10\%$.

3. MAGNITUDE EQUALISER—A GROUP OF ‘PHANTOM ZEROS’

3.1. APPLICATION OF THE FINITE ELEMENT METHOD IN EXTRACTION OF ‘PHANTOM ZEROS’

The method proposed in reference [2] to obtain a group of ‘phantom zeros’ for compensation of truncation was to make an initial measurement of the true FRF [2, 3], meaning that the response and excitation need to be measured simultaneously. Measuring the excitation may be very difficult in many cases, even when the investigated machine is not in operation. In such cases, it may be possible to get a good estimate of the true FRF rather than measure it. In the following we will examine how the finite element method (FEM) can be applied to construct a valid FRF, and then how ‘phantom zeros’ can be extracted from such constructed FRFs.

The free-free beam shown in Fig. 3 (without slot) was used for this purpose. The beam was divided into 28 equal divisions in its axial direction and two equal divisions in the

TABLE 1
Shift of the pole positions (Hz)

Slot depth (mm)	Pole 1	Pole 2	Pole 3	Pole 4	Pole 5	Pole 6	Pole 7	Pole 8
0	$-2.61 \pm j100.3$	$-3.65 \pm j274.7$	$-4.12 \pm j536.8$	$-3.58 \pm j883.4$	$-3.45 \pm j1311$	$-3.59 \pm j1819$	$-3.79 \pm j2404$	$-4.23 \pm j3062$
2	$-3.45 \pm j99.77$	$-3.84 \pm j275.2$	$-4.06 \pm j535.6$	$-3.62 \pm j883.5$	$-3.19 \pm j1308$	$-3.48 \pm j1819$	$-3.36 \pm j2398$	$-4.26 \pm j3062$
4	$-3.24 \pm j98.82$	$-4.15 \pm j275.4$	$-3.78 \pm j531.8$	$-3.70 \pm j883.7$	$-3.05 \pm j1300$	$-3.50 \pm j1820$	$-3.33 \pm j2382$	$-4.43 \pm j3062$
6	$-3.31 \pm j97.24$	$-3.65 \pm j275.1$	$-3.67 \pm j524.9$	$-3.60 \pm j883.7$	$-3.05 \pm j1285$	$-3.44 \pm j1820$	$-3.11 \pm j2351$	$-3.94 \pm j3062$
8	$-3.99 \pm j94.67$	$-3.78 \pm j274.9$	$-3.28 \pm j515.4$	$-3.82 \pm j883.7$	$-2.92 \pm j1263$	$-3.56 \pm j1820$	$-3.77 \pm j2299$	$-5.57 \pm j3061$
10	$-2.80 \pm j90.11$	$-3.32 \pm j276.0$	$-3.50 \pm j501.1$	$-3.36 \pm j884.0$	$-2.99 \pm j1232$	$-3.91 \pm j1820$	$-3.15 \pm j2222$	$-5.30 \pm j3061$

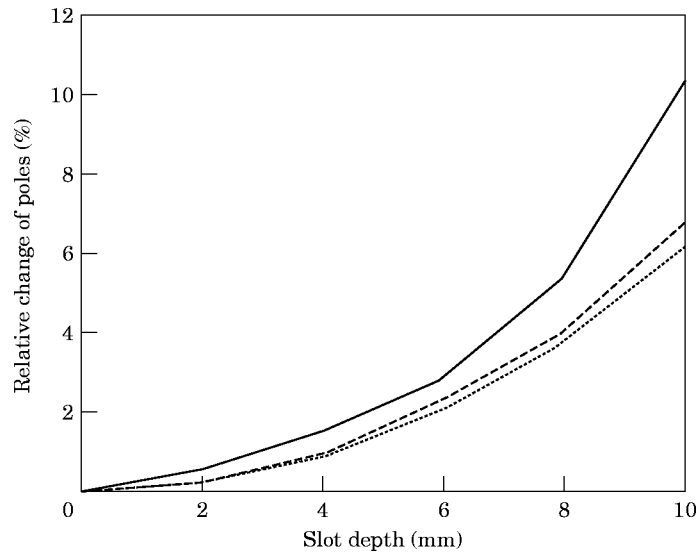


Figure 5. Relative shift of the symmetric modes. —, Pole 1; ---, pole 3;, pole 5.

other two directions in its cross sectional plane, thus giving a finite element model of the beam with 112 brick elements, each of which has eight nodes. The node freedoms allowing lateral bending vibration at the vertical plane of symmetry of the beam were inhibited, since only the vertical bending vibration is of interest here. The software package of Strand 6.0 [11] was used to establish the model and calculate the dynamic properties. In the calculation, the number of modes was set to 10 and use was made of a feature of Strand 6.0 which enables the user to specify a frequency shift in the eigenvalue problem [11] (to avoid calculating all the rigid body modes in the case where the object is not fully restrained). Among the 10 modes calculated, there were eight bending modes, one rigid body mode and one longitudinal (axial) mode. In constructing FRFs of the beam bending vibration, the longitudinal mode was removed because it contributed nothing to the bending vibration. Likewise, the rigid body mode, which was a linear combination of translation and rotation, was not used, as the calculable zero frequency value of acceleration (see later, Section 4.1) was used to generate each FRF.

TABLE 2
Frequencies and mode shapes obtained by FEM

Frequency (Hz)	FEM results Mode shapes			Theoretical frequency (Hz)	Measured frequency (Hz)
	Point 1	Point 5	Point 8		
100.89	-1.6786	0.94482	-1.6772	98.9	100
277.18	1.6660	0.60810	-1.6650	272.6	276
541.80	-1.6489	-0.84972	-1.6502	534.6	536
893.11	-1.6297	0.91340	1.6282	883.8	884
1330.2	1.6017	-0.39766	1.6030	1320	1312
1853.5	-1.5706	-1.1524	1.5700	1843	1820
2460.8	-1.5318	0.10630	-1.5313	2454	2404
3154.1	-1.4850	1.0927	1.4866	3151	3064

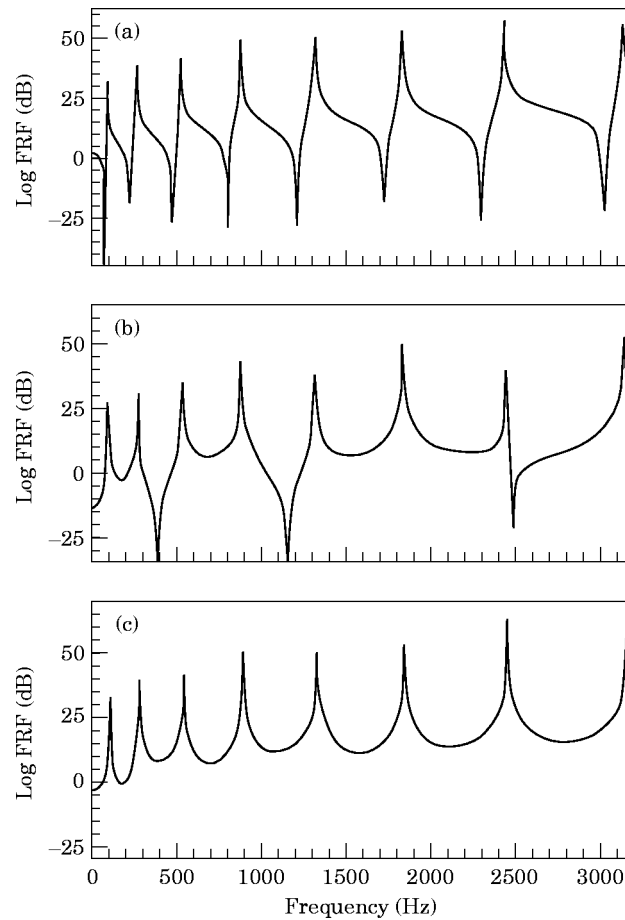


Figure 6. FRFs constructed using the modal parameters obtained by FEM. (a) Point 1; (b) point 5; (c) point 8.

Table 2 lists the natural frequencies and the mode shape components corresponding to the three points 1, 5 and 8, and for comparison shows the theoretical (Euler–Benoulli theory) and measured frequencies. It can be seen that the three sets of frequencies correspond well but not exactly.

The model parameters in Table 2 were used to construct the FRFs in terms of the pole/residue model for zero damping [14, 1]. Figure 6 illustrates the (log) FRFs constructed in such a way. Compared with the measured FRFs (dashed curves in Fig. 1), the following can be seen, (a) the positions of the poles and zeros in Figs 1 and 6 correspond well, meaning that the poles and zeros obtained by the FEM could be used as the initial values in the NLLS optimisation procedure, and (b) the general slopes of the (log) FRFs measured and constructed according to the modal parameters from the FEM are the same. This indicates that it is possible to use such constructed FRFs to correct the deviation of the general slopes caused by truncation (solid curves in Fig. 1). Note that the peaks and valleys in Fig. 6 are sharper than those in Fig. 1 because the FRFs in Fig. 6 were generated using the modal parameters without damping. In practice a small amount of proportional damping could be added to avoid problems with frequency samples close to poles and zeros, but the damping does not affect the general slope of the FRFs.

The distributions of the ‘phantom zeros’ for three points considered here are illustrated in Fig. 7. The ‘phantom zeros’ were obtained by curvefitting the FRF (in the frequency range 0–1500 Hz) in Fig. 6 using the rational fraction polynomial (RFP) curvefitter [5]. All the ‘phantom zeros’ are symmetric about both the frequency and damping axes.

Figure 8 shows the resultant magnitude compensations corresponding to the ‘phantom zero’ groups in Fig. 7. Excellent correspondence can be found between any one of the curves of Fig. 11 (based on measurements) and Fig. 8. For point 1, the resultant compensation is nearly flat in the frequency range up to 900 Hz, and there is a small deviation beyond 900 Hz. For points 5 and 8, the resultant compensations are nearly straight lines (except in the very low frequency region), having the same general slopes in Fig. 8(b) and (c) as in Fig. 11(b) and (c), respectively.

Figure 9 illustrates the measured FRFs (dashed curves) and the FRFs (solid curves) generated by cascading the true physical poles and zeros (extracted through curve-fitting response cepstra) with the ‘phantom zero’ groups in Fig. 7. Note that as explained in [2] the number of phantom zeros required is greater the greater the separation of the excitation and response points, because of the reduced proportion of true zeros (antiresonances). In this case, the generated FRFs are scaled by the mean values of the log FRFs (see later). It can be seen that the same goodness of match between the dashed and solid curves in Fig. 9 can be achieved by adding the ‘phantom zeros’ obtained from the FEM as by adding the ‘phantom zeros’ obtained from curvefitting the measurements of true FRFs, for which the combined results are shown in Fig. 14.

3.2. OUT-OF-BAND MODE CONTRIBUTIONS WITH SLOT DEVELOPMENT

As mentioned above, the magnitude equaliser is used to compensate for the distortion of the general slope caused by truncation [1, 2]. The problem here is the question of how the in-band contribution of out-of-band modes changes with the slot development. At the beginning, we have argued that the in-band contribution of the out-of-band modes remains nearly unchanged with slot development, and that it mainly affects the general slope of the in-band (log) FRF. These assumptions will be examined in this section.

In order to tackle this problem, the FRF data measured on the free-free beam with 2 mm slot depth increments (up to 10 mm deep) were curve-fitted using the RFP curve-fitter. For the three measurement points (1, 5 and 8), the ‘phantom zero’ groups

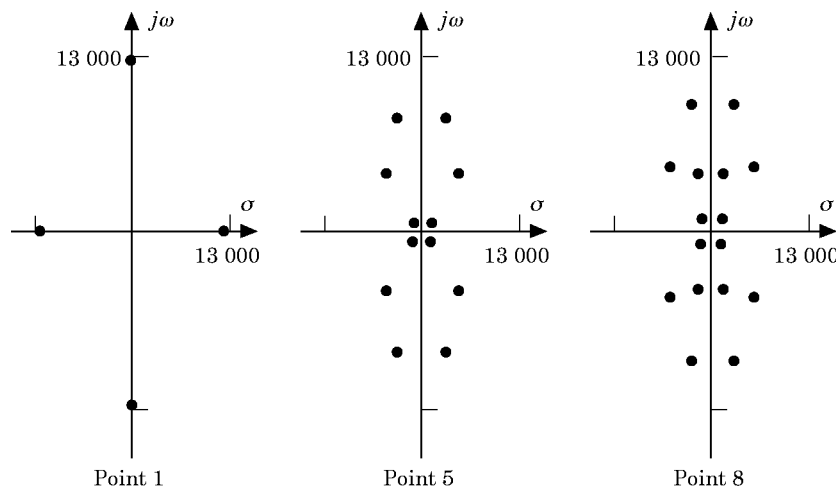


Figure 7. Distribution of the ‘phantom zeros’ obtained by curve-fitting the FRFs in Fig. 6.

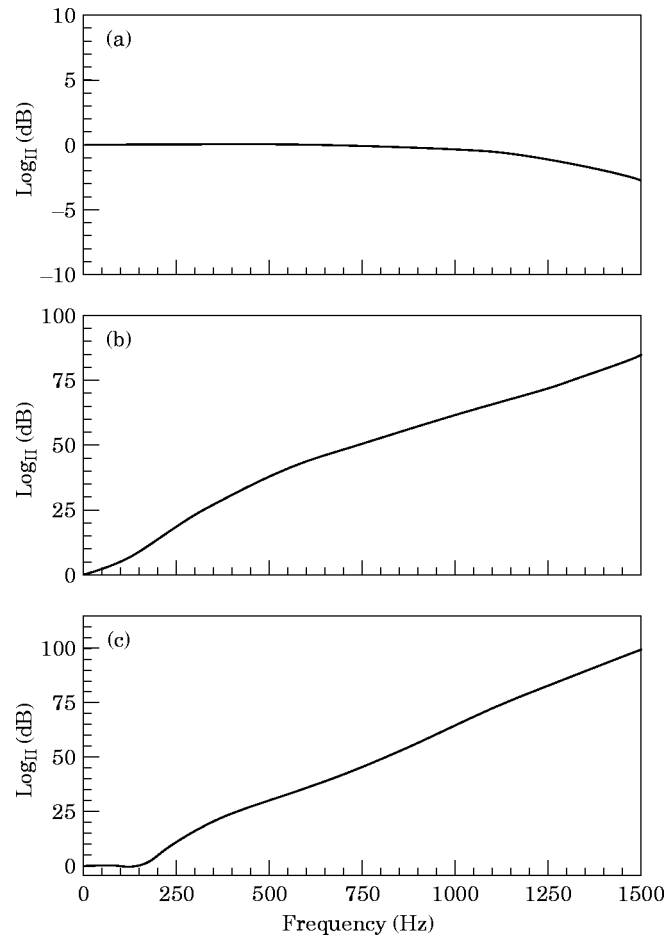


Figure 8. Resultant log magnitudes of the 'phantom zero' groups in Fig. 7. (a) Point 1; (b) point 5; (c) point 8.

corresponding to different slot depths were identified. Figure 10 shows some typical distributions of such 'phantom zero' groups for point 5, with Figs 10(a)–(c) corresponding to the 0, 4 and 8 mm slot depths on the beam, respectively. It can be seen that the distributions of the 'phantom zeros' in the Laplace plane are different, but their patterns are similar. From the point of view of compensation for the distortion of general slope, we are more interested in the resultant overall contribution as a magnitude equaliser, rather than the individual patterns (distributions) of the group of 'phantom zeros'. Figure 11 illustrates the resultant contributions of the 'phantom zero' groups corresponding to the slot depth of 0, 2, 4, 6, 8 and 10 mm for the three measurement points, respectively. All the curves in the three figures are scaled to 0 dB at 0 Hz for convenience of comparison, and in each case the curve for zero slot depth is shown in full with the others dashed.

Figure 11(a) compares the resultant contributions among the six cases of different slot depths at the driving point (point 1). The six curves are quite flat in the lower frequency band ($f < 900$ Hz) and their slopes become steeper in the higher frequency section ($f > 900$ Hz). This is a characteristic of the contribution of the out-of-band modes at the driving point. The out-of-band zeros and poles appear alternately in a driving point measurement. Their modulus ratios tend to balance when the test frequency, ω , is far from them, which results in the flat curve in the lower frequency section. However, the modulus

ratio deviates from unity when the test frequency, ω , comes closer to them (in our case, when ω is close to the right end of the frequency band), which makes the curves in the higher frequency section steeper. By inspecting the relative positions of the six curves, it can be seen that there is no trend in the curve shifts (or variation of the curve relative positions), with slot development. The deviations of the other five curves from the solid curve (corresponding to no slot on the beam) are presumably caused by curve fitting errors. The maximum deviation is about 0.7 dB (8% relative error), which is obtained at the upper end of the frequency band. The above deviation can be further reduced if the curves are scaled to other than the zero frequency values.

Figures 11(b) and (c) compare the resultant contributions of the 'phantom zero' groups obtained from the measurements at points 5 and 8, respectively. It is hard to find any trend of these compensation curves with the slot development. All the curves in each figure are parallel except at the very beginning of the frequency band ($f < 75$ Hz). The six curves in Figs 11(b) or (c) have the same general slopes within the frequency range, 0–1500 Hz, and the deviations are presumably due to the curve fitting errors at low frequency as discussed below.

A very significant result from the above discussion is that any one of the six curves in Figs 11(a), (b) or (c) (or the corresponding one obtained from the FEM model in Fig. 8)

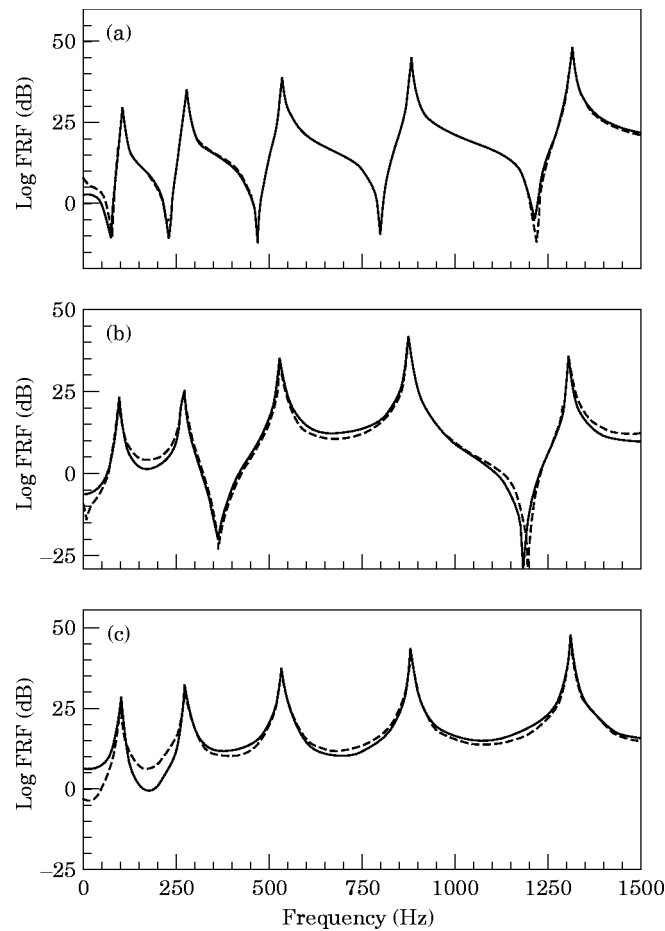


Figure 9. Compensation effects of the 'phantom zero' groups in Fig. 7. (a) Point 1; (b) point 5; (c) point 8.

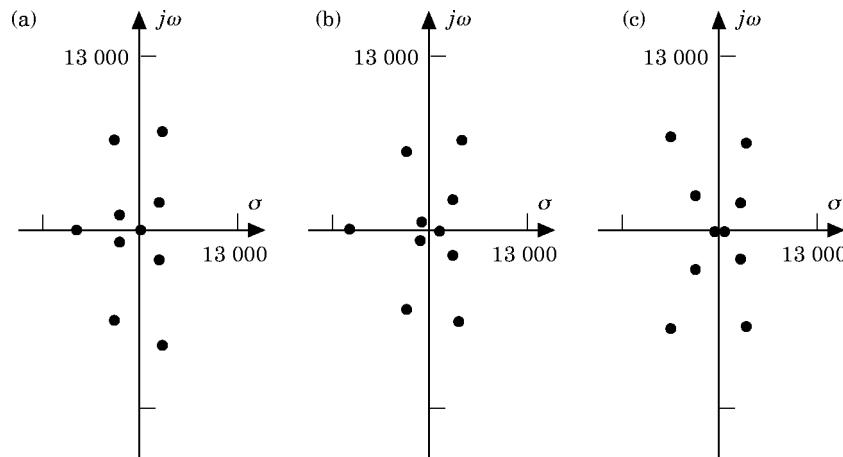


Figure 10. Distribution of 'phantom zeros' at point 5 with slot depths, 0, 4 and 8mm.

can be used to replace the other five in order to correct the distortion of the general slopes of the in-band (log) FRFs. This result is very useful in practice. The pre-determined magnitude equaliser (corresponding to the solid curves in Figs 11 or 8) can be used to compensate for the truncation effect even as the FRF changes (slot development in our case). It seems that this result can be used to a quite large extent of change. In our case, the beam cross section was reduced to 48% of its original value (although the width of the slot would also have considerable effect) and natural frequencies changed by as much as 10%.

4. SCALING THE REGENERATED FRFs

It has been shown that the truncated pole/zero model, cascaded with a magnitude equaliser, can determine an FRF to within a scaling factor [1–3]. It may not be so important to scale the overall FRF function absolutely for some diagnostic applications, as in the case where only the relative change of the resonance positions is concerned. On the other hand, however, it becomes necessary to scale an FRF in absolute terms when it is to be used as an inverse filter in order to recover the vibration sources [12, 13], or used to predict the vibration level due to a given force. This section examines how to scale an FRF regenerated by the above model.

4.1. SCALING IN TERMS OF RIGID BODY MOTION INERTIA

Theoretically, it should be possible to scale the overall FRF (accelerance) to the value at zero frequency, the component of which represents the rigid body motion inertia of a free-free structure, such as the beam considered here. The zero frequency component of an FRF (accelerance) at a given measurement point is the acceleration at that point due to unit load on the structure. Generally, the acceleration is the superposition of the translation at the centre of gravity and the rotation around it and can be calculated from a knowledge of the inertial properties. As an example, the response accelerations measured at point 1 on the free-free beam are $4/m$, $4/7m$ and $-2/m$ under unit force excitation at points 1, 5 and 8, respectively. Here, m is the total mass of the beam. Figure 12 shows the calculation procedure.

In principle, a local material damage, such as the slot development in the beam, might cause considerable change in its distributed stiffness, but the change of rigid body motion

inertia can be neglected in practice, as with the beam slot, where the inertia loss, compared with the total inertia of the beam is very small. So, the above three scaling factors (Fig. 12) could be used to scale the FRFs with or without a slot in the beam. The same should apply in most cases where the primary change in the FRF is due to changes in stiffness rather than inertia.

Figure 13 illustrates two extreme cases, (a)–(c) correspond to no slot on the beam, and (d)–(f) to a 10-mm deep slot for points 1, 5 and 8, respectively. The scaling at point 1 is excellent for both cases [(a) and (d)], but it becomes poorest at point 5 [(b) and (e)]. The scaling at point 8 is good for the no slot case but not so good for the 10-mm slot case.

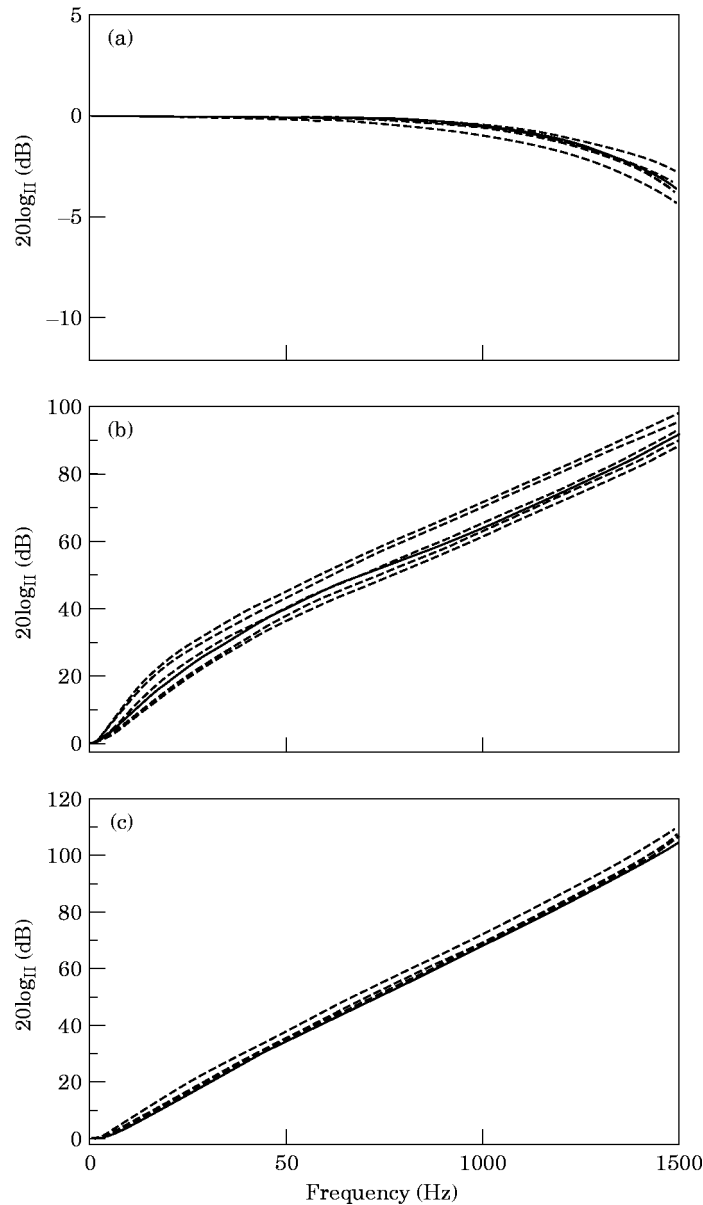


Figure 11. Resultant compensation of 'phantom zeros' for truncation at (a) point 1; (b) point 5 and (c) point 8. —, zero slot depth; ---, other slot depths.

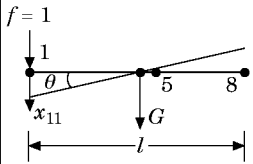
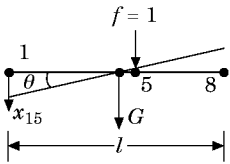
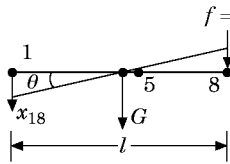
Point 1	Point 5	Point 8
		
$\ddot{x}_{11} = \frac{1}{m} + \frac{\ddot{\theta}_{11}l}{2} = \frac{4}{m}$	$\ddot{x}_{15} = \frac{1}{m} - \frac{\ddot{\theta}_{15}l}{2} = \frac{4}{7m}$	$\ddot{x}_{18} = \frac{1}{m} - \frac{\ddot{\theta}_{18}l}{2} = -\frac{2}{m}$

Figure 12. Zero frequency components at points 1, 5 and 8.

The above scaling deviation is thought to be due to the sensitivity of the method to the goodness of fit to the very low frequency components, which is the chief drawback of this method which scales the overall FRF according to only a single (zero) frequency component. It is a feature of the rational fraction polynomial (RFP) method [5] that it minimises the error primarily of the largest components in the FRF, and in particular with accelerance measurements the deviation is greatest at low frequency. It is possible that by fitting the FRF in terms of velocity or displacement, the low frequency error would be reduced, in which case the scaling in terms of the zero frequency value would be improved.

4.2. SCALING IN TERMS OF THE MEAN VALUES OF LOG FRFS

The mean value of a log spectrum reflects the corresponding scaling factor in the way that both of them represent the vertical translation of the overall log FRF. So it is convenient to scale the FRF with the mean value obtained from the pre-measurement if the variation of the actual mean value falls within an acceptable range with the damage development. This is true especially for free-free structures with crack development. Firstly, the change of inertia (or mass distribution) in the structure considered is either negligible (as with the beam slot) or equal to zero (without mass loss as with a crack), meaning that the zero frequency component would remain the same, as discussed above. Secondly, local material damage would not greatly change the general slopes of the log FRFs, as illustrated in Fig. 11. Lastly, local material damage does shift the positions of the poles and zeros, which could result in the variation of some frequency components, especially those around peaks and valleys. However, the effect of such variation on the corresponding mean value over the whole spectrum is very small, as illustrated by the current example.

In order to evaluate the variation of the mean value of the log FRFs in the frequency range 0–1500 Hz, Table 3 lists them for the three measurement points with slot development in the beam. It can be seen that the mean values at each point are nearly the same, the maximum deviation from the initial measured value being 0.83 dB at point 8 when the slot is 6 mm deep. Figure 14 shows the correspondence between the measured (dashed lines) and the regenerated FRFs (solid lines) which are scaled by the mean values in the first column of Table 3. For the two extreme cases (0 and 10 mm deep slots) and all three measurement points, the dashed and solid curves match each other very well.

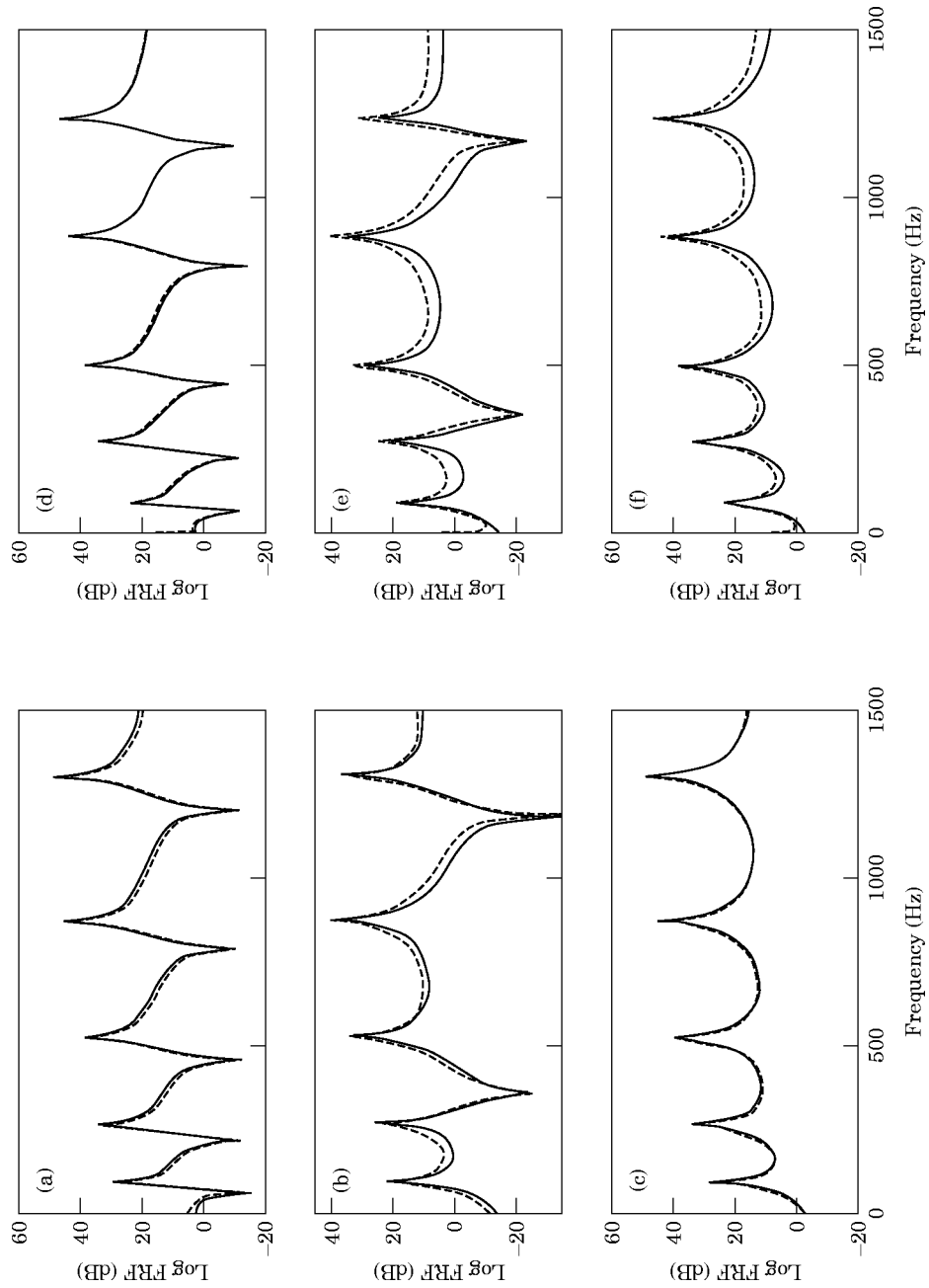


Figure 13. Scaling FRF in terms of rigid body motion inertia (a)–(c) no slot; (d)–(f) 10-mm slot. —, Regenerated; ---, measured.

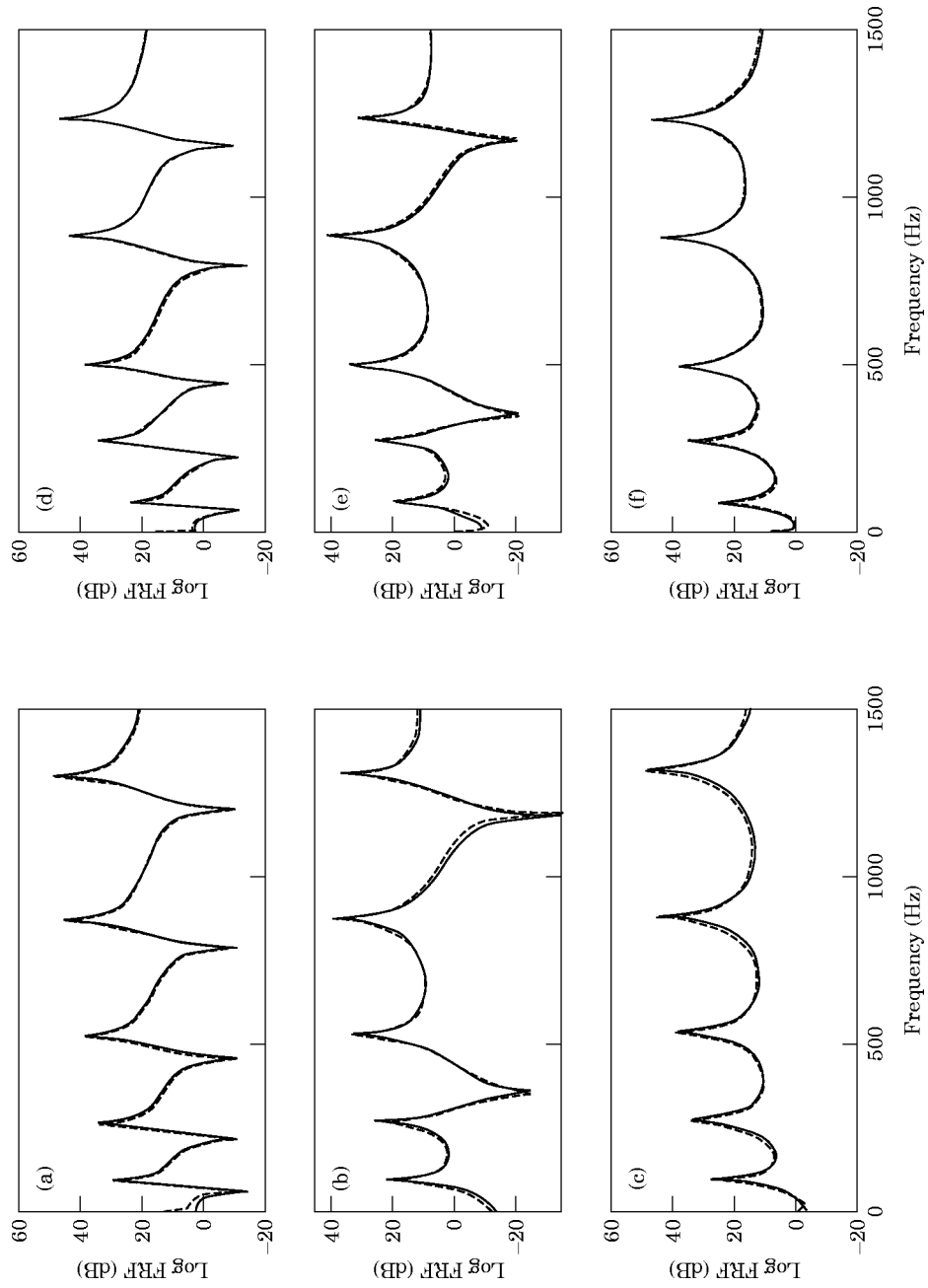


Figure 14. Scaling FRF in terms of the mean values of log FRF (a)–(c) no slot; (d)–(f) 10-mm slot. —, Regenerated; ----, measured.

4.3. SCALING IN TERMS OF THE PREDETERMINED SCALING FACTORS

Based on the same principle as above, the overall log FRF regenerated from the curve-fitted poles and zeros (including ‘phantom zeros’), with damage development, could be scaled by the scaling factor obtained from the curve fitting process together with the corresponding magnitude equaliser from initial measurements (or FEM model). For example, the three scaling factors obtained from the three initial measurements (points 1, 5 and 8 without slot) at the same time as the solid lines in Fig. 11 are -3.31 , -1.84 and 1.97 , respectively. Figure 15 illustrates the goodness of the above three scaling factors for the two extreme cases. The dashed lines are the measured ones and the solid lines the regenerated (same poles and zeros are used as for the regenerated curves in Fig. 14).

The following comments can be made on the above scaling methods. (1) The rigid body motion inertia scales the FRFs according to one frequency component only (at zero or a frequency very close to zero), and their scaling accuracy depends on the goodness of that component relative to the overall FRF. This means that a possible local deviation of the regenerated FRF in the low frequency region can lead to an appreciable scaling error. (2) The mean logarithmic values and predetermined scaling factor scale the FRFs in terms of all the frequency components in the whole frequency range, and their scaling accuracy should be better than that of the rigid body motion inertia. (3) As might be expected, the results using a predetermined scaling factor tend to be dominated by the largest peaks, where the curve fitting is most accurate.

4.4. SCALING FOR CONSTRAINED STRUCTURES

For a constrained structure, the FRF (receptance) would tend to a constant stiffness at zero frequency. Unfortunately, a small local material damage in a continuous structure may result in a very large variation of its static stiffness, meaning that the initially determined stiffness can not be used to scale the FRF with the damage development (though the change in static stiffness could possibly be measured by applying a static load at the excitation point and measuring the displacement at the point where the FRF is scaled). On the other hand, it could be possible to scale the (log) FRFs according to the mean values or the predetermined scaling factors in the situation where the mode shapes of the structure at the initial stage are still good approximations to those with damage development. The reason is that the local material damage does not change the mass distribution of the structure considered and the mass line [14] for each mode would remain nearly the same. The changes in resonances and antiresonances by up to 10%, and corresponding shifts in the stiffness lines should not affect the mean amplitudes of the FRFs greatly, as with unconstrained structures.

TABLE 3
Mean values of the FRFs with slot development (dB)

	Slot depth (mm)					
	0	2	4	6	8	10
Point 1	15.21	14.86	14.97	14.64	15.08	15.62
Point 5	8.06	7.97	7.71	7.39	8.08	8.28
Point 8	17.10	17.01	16.65	16.27	16.77	17.14

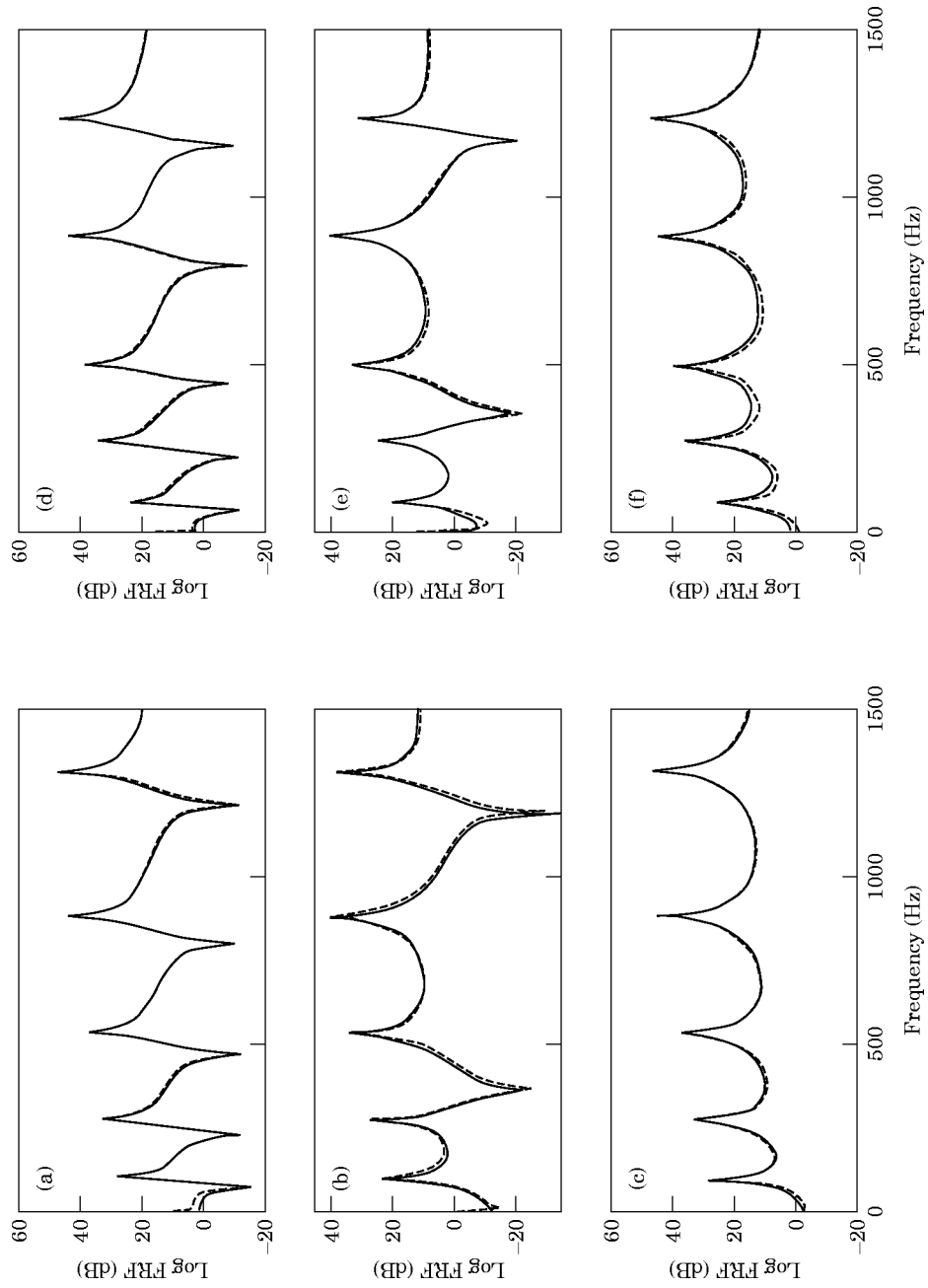


Figure 15. Scaling FRF in terms of the predetermined scaling factors (a)–(c) no slot; (d)–(f) 10-mm slot. —, Regenerated; ----, measured.

5. REGENERATION OF FRFs WITH SLOT DEVELOPMENT

Figures 13–15 show the goodness of the FRF models constructed using the true in-band poles and zeros (tracked using the NLLS or ITD methods) cascaded with the pre-determined magnitude equalisers. Figure 16 regenerates the FRFs at the three points with slot development in the beam to illustrate the amount of change which has been accommodated. All the FRF curves are obtained by cascading the truncated pole/zero model with a magnitude equaliser (solid curves in Fig. 11) and then scaled by the three predetermined scaling factors (as in Fig. 15).

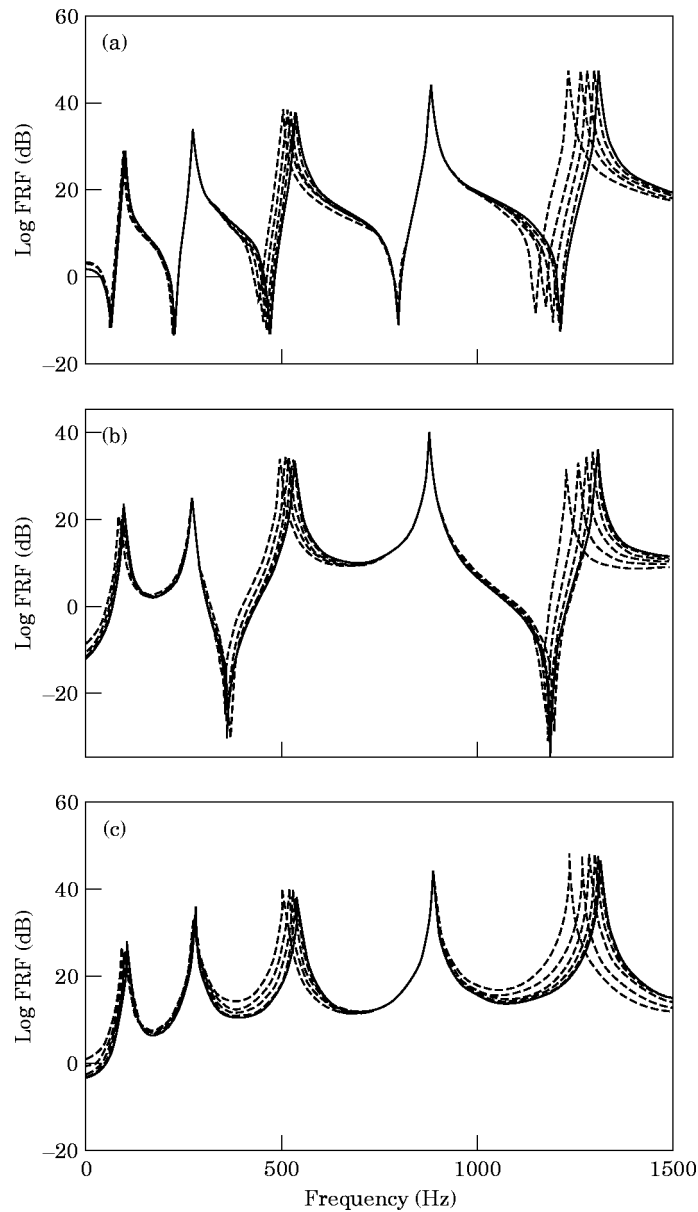


Figure 16. Regeneration of FRFs with slot development. (a) Point 1; (b) point 5; (c) point 8.

The relative position change between pole and pole, pole and zero or zero and zero could be used indirectly to evaluate the change of the corresponding residues. The pole/zero model implies that if a zero is shifted very close to a pole, the vibration strength of that pole (residue) would be decreased, and vice versa. In Fig. 16(a), for the driving point, the relative positions between the pole of a symmetric mode and the zero just before it remains nearly the same, as do the corresponding peak values with slot development. In Fig. 16(b), for point 5, the fifth peak value becomes smaller and smaller when the zero just to the left of it approaches the pole with slot development. Note that point 5 is closest to the slot, and point 1 the most remote.

6. CONCLUSIONS

Out-of-band modes contribute mainly to the general slope of the in-band FRF. This contribution remains nearly unchanged with local material damage development in a structure (though the out-of-band poles and zeros might shift), meaning that a group of predetermined 'phantom zeros', functioning as a magnitude equaliser, can be used to compensate for the contribution of the out-of-band modes. The magnitude equaliser can be determined from either pre-measurement of true FRFs or from a finite element model.

The FRF can be regenerated to within a scaling factor by cascading the true physical poles and zeros, tracked with damage development by curve-fitting the path dominated part of the complex or differential cepstra, with a magnitude equaliser. The scaling factor can be based on the rigid body motion inertia, the mean value of the (log) FRF, or determined during the curve fitting process together with the magnitude equaliser. It was found that the scaling accuracy given by the rigid body inertia is poorer than the other two factors since it is based on only one frequency component and because the Rational Fraction Polynomial curvefitting technique gives largest errors at low frequency on acceleration measurements.

The procedure for regeneration of updated FRFs as they change is carried out recursively with updated true physical poles and zeros from response cepstra without the necessity of measuring the forcing function. This has been found to be valid at least for the type of changes investigated here; a slot of increasing depth giving rise to changes in natural frequencies of up to 10 per cent.

The regenerated FRFs could be used in an inverse filtering process to obtain better estimates of the forcing functions than would result from assuming no change in the structural properties. They could also be used to adapt to changes in response properties due to different operating conditions, for example where it might be possible to make measurements of FRFs on a machine which is stationary, and then adjust to operating conditions. The method could also be used to measure the variability in structural dynamic properties between machines and structures made to the same design, and thus having the same properties according to a finite element model. It has been demonstrated that such a finite element model can be used as an alternative to an initial measurement to provide amplitude equalisers and scaling factors which do not vary greatly with limited material damage or variation between units. The method has considerable application where it is difficult or impossible to measure the forces applied during operation.

ACKNOWLEDGMENTS

The authors would like to thank Professor Aldo Sestieri and Dr Antonio Carcaterra of the University of Rome for providing the RFP curve fitting program. This research was supported by an Australian Research Council grant.

REFERENCES

1. Y. GAO 1994 *PhD lissertation*, University of New South Wales, Australia. Extraction of modal parameters from response vibrations.
2. R. B. RANDALL, Y. GAO and A. SESTIERI 1992 *Proceedings of the 17th International Seminar on Modal Analysis*, K. U. Leuven, Belgium, 503–517. (Modified version published in *Mechanical Systems and Signal Processing* 1994 **8**, 607–622). Phantom zeros in curve-fitted frequency response functions.
3. R. B. RANDALL and Y. GAO 1994 *Journal of Sound and Vibration* **176**, 179–193. Extraction of modal parameters from the response power cepstrum.
4. Y. GAO and R. B. RANDALL 1996 *Mechanical Systems and Signal Processing* **10**, 293–317. Determination of frequency response functions from response measurements—Part 1. Extraction of poles and zeros from response cepstra.
5. M. H. RICHARDSON and D. F. FORMENTI 1985 *Proceedings of the 3rd IMAC*, Orlando, FL, 390–397. Global curve-fitting of frequency response measurements using the rational fraction polynomial method.
6. J. K. VANDIVER 1977 *Journal of Petroleum Technology*, 305–310. Detection of structural failure on fixed platforms by measurement of dynamic response.
7. J. C. S. YANG *et al.* 1980 *Computation Methods for Offshore Structures*, ASME Publications AMD37, 55–68. Application of the random decrement technique in the detection of an induced crack on an offshore model.
8. W. T. THOMSON 1949 *Journal of Mechanics* **16**, 203–207. Vibration of slender beams with discontinuities.
9. A. JOSHI *et al.* 1991. *Journal of Sound and Vibration* **147**, 475–488. A unified approach to free vibration of locally damaged beams having various homogeneous boundary conditions.
10. M. M. F. YUEN 1985 *Journal of Sound and Vibration* **103**, 301–310. A numerical study of the eigen parameters of a damaged cantilever.
11. G + D computing Pty. Ltd., Ultimo, Australia 1991 *Strand 6.0, User Manual and Reference Guide*.
12. A. V. OPPENHEIM and R. W. SCHAFER 1989 *Discrete Time Signal Processing*. Englewood Cliffs, NJ: Prentice-Hall.
13. R. H. LYON 1987 *Machinery Noise and Diagnostics*. London: Butterworth.
14. D. J. EWINS 1989 *Modal Testing: Theory and Practice*, Letchworth: Research Studies Press.